

X-ray variability with spectral state transitions in NS-LMXBs observed with MAXI/GSC and Swift/BAT

Kazumi ASAI,¹ Tatehiro MIHARA,¹ Masaru MATSUOKA,¹ and Mutsumi SUGIZAKI,¹

¹MAXI team, RIKEN, 2-1 Hirosawa, Wako, Saitama 351-0198
kazumi@crab.riken.jp

(Received 2015 April 19; accepted 2015 June 5)

Abstract

X-ray variabilities with spectral state transitions in bright low mass X-ray binaries containing a neutron star are investigated by using the one-day bin light curves of MAXI/GSC (Gas Slit Camera) and Swift/BAT (Burst Alert Telescope). Four sources (4U 1636–536, 4U 1705–44, 4U 1608–52, and GS 1826–238) exhibited small-amplitude X-ray variabilities with spectral state transitions. Such “mini-outbursts” were characterized by smaller amplitudes (several times) and shorter duration (less than several tens of days) than those of “normal outbursts.” Theoretical model of disk instability by Mineshige and Osaki (PASJ, 37, 1, 1985) predicts both large-amplitude outbursts and small-amplitude variabilities. We interpret the normal outbursts as the former prediction of this model, and the mini-outbursts as the latter. Here, we can also call the mini-outburst as “purr-type outburst” referring to theoretical work. We suggest that similar variabilities lasting for several tens of days without spectral state transitions, which are often observed in the hard state, may be a repeat of mini-outbursts.

Key words: accretion, accretion disks — stars: neutron — X-rays: binaries

1. Introduction

The X-ray spectra of low mass X-ray binaries with a neutron star (NS-LMXBs) mainly depend on the X-ray luminosities (e.g., Lewin et al. 1997). High luminosity ($\gtrsim 10^{37}$ erg s^{−1}) dominated by thermal component is called “soft state,” whereas low luminosity ($\lesssim 5 \times 10^{36}$ erg s^{−1}) dominated by the Comptonized component is called “hard state.” In general, the luminosity is thought to reflect the mass-accretion rate and then the spectral state (soft or hard) corresponds to a state of the inner accretion disk (optically thick or thin) (e.g., Mitsuda et al. 1989; White et al. 1988; Done et al. 2007; Matsuoka & Asai 2013). Spectral states are a key to determine the state of the inner accretion disk.

Bright NS-LMXBs have been classified into two groups, Z sources and Atoll sources, based on their behavior on the color–color diagram and hardness–intensity diagram (Hasinger & van der Klis 1989). Z sources are generally bright and sometimes become close to the Eddington luminosity (L_E). On the other hand, Atoll sources are generally less bright, and some of them exhibit spectral state transitions (soft or hard). In the color–color diagram, the shape can be divided into two main regions, “banana” and “island.” The spectrum is usually softer in the banana than in the island.

Spectral state transitions have been studied for transient X-ray binaries including a neutron star or a black hole (e.g., Maccarone 2003; Maccarone & Coppi 2003; Yu & Yan 2009; Tang et al. 2011; Asai et al. 2012). Usually, these transitions are observed in the rise and decay phases of outbursts, when the luminosity changes by 2–5 orders of

magnitude during outbursts. Maccarone (2003) reported that the soft-to-hard transition in the decay phase of the outburst occurs at 1%–4% of L_E . For the hard-to-soft transition in the rise phase of the outburst, the transition luminosity tends to be larger than that in the soft-to-hard transition (Miyamoto et al. 1995; Maccarone & Coppi 2003; Asai et al. 2012). The spectral state transitions have been also observed in four persistent NS-LMXBs: 4U 1636–536 (Shih et al. 2005), GS 1826–238 (Nakahira et al. 2014), 4U 1705–44 (Lin et al. 2010), and 4U 1820–30 (Wen et al. 2006; Titarchuk et al. 2013). The X-ray variability with spectral state transitions means the change of the intrinsic mass accretion rate.

Recurrent outburst behavior is interpreted by the thermal viscous disk instability model (see Lasota 2001 for a review). In this model, local disk instabilities (S-shaped curves in the surface density and mass accretion rate diagram) are caused by the partial ionization of hydrogen and helium. The local instabilities propagate over the whole disk, and when it reaches the innermost part of the accretion disk, an outburst occurs. Mineshige and Osaki (1983, 1985) investigated the disk instability model for outbursts of dwarf novae. They reported that instabilities on a constant- α disk yield only small-amplitude variabilities, where α is the standard viscosity parameter. This was also pointed out by Smak (1984) and Meyer (1984). On the other hand, by assigning high α in a hot state (upper branch in S-shaped curve) and low α in a cool state (lower branch), the width of the unstable branch (middle branch) is extended and the instability can propagate through the whole disk. The two- α disk leads to the large-amplitude outbursts. Mineshige and Shields (1990a) studies the sim-

ilar variability for the disk instability in AGN, and then, they named the small and the large amplitude variabilities as “purr type” and “roar type,” respectively. In this paper, we propose that some small amplitude variabilities (mini-outbursts) detected in NS-LMXBs are considered to be the purr-type outburst.

Smak (1982, 1983) showed that instability occurs below a critical effective temperature depending on the mass accretion rate. They classified the cataclysmic variables into two objects on the outer disk radius versus mass accretion rate diagram: stationary-accretion objects (novae and nova-like stars) and non stationary-accretion objects (dwarf novae). External heating by central object may be ignored in white dwarfs, but is non-negligible in NS-LMXBs because the disk is strongly irradiated. In other words, instability is determined by not only the mass accretion rate, but also the X-ray luminosity. Tuchman, Mineshige, and Wheeler (1990) calculated the instability in consideration of the effect of irradiation, and generated the S-shaped curves at different irradiation temperatures. They concluded that for sufficiently strong irradiation (irradiation temperature above 10000 K), the hydrogen and helium atoms are completely ionized, thus, the thermal instability is suppressed. van Paradijs (1996) also calculated the effect of external heating and separated persistent NS-LMXBs from transient NS-LMXBs on the orbital period versus X-ray luminosity diagram.

The present study focuses on the properties of the spectral state transitions of transient and persistent NS-LMXBs. The analyzed data are MAXI (Matsuoka et al. 2009)/GSC (Gas Slit Camera: Mihara et al. 2011; Sugizaki et al. 2011)¹ and Swift (Gehrels et al. 2004)/BAT (Burst Alert Telescope: Barthelmy et al. 2005)² from 2009 August 15 (MJD = 55058) to 2014 December 31 (MJD = 57022). Section 2 describes the data analysis and the properties of spectral state transition. In section 3, we discuss the properties of the transition based on the disk instability model. Conclusion is presented in section 4.

2. Analysis and results

2.1. Source selection

We investigated spectral state transitions in bright NS-LMXBs using the one-day bin light curves of MAXI/GSC and Swift/BAT. The hardness ratio of BAT (15–50 keV) and GSC (2–10 keV) is suitable for identifying spectral state transitions in NS-LMXBs, as was employed by Yu and Yan (2000), Tang, Yu, and Yan (2011), and Asai et al. (2012). The obtained count rates of GSC and BAT were converted to luminosities by assuming a Crab-like spectrum (Kirsch et al. 2005) and the distances listed in the LMXB catalogue (Liu et al. 2007).³ This assumption is

acceptable in the hard state, because the energy spectrum is dominated by the Comptonized emission approximated by a power-law. On the other hand, in the soft state, the energy spectrum is dominated by the thermal emission. The obtained luminosity by assuming Crab-like spectrum is underestimated in the 2–10 keV band and is overestimated in the 15–50 keV band. When the spectrum in the soft state is a blackbody emission with $kT \sim 2\text{--}2.5$ keV, the obtained luminosity in the 2–10 keV band is 0.7 of that of the blackbody emission. In the 15–50 keV, the obtained luminosity is 1.4 of that of the blackbody emission. As a result, the hardness ratio of two energy bands is overestimated by 2.0 times. Moreover, we need a bolometric correction to discuss the luminosities. The correction factor from a 2–10 keV luminosity to a bolometric (0.1–100 keV) one is 1.4–1.7 for the blackbody spectrum assumed above. In this paper, those corrections should be considered to discuss the real luminosity.

We identified the spectral state transition from the BAT/GSC hardness ratios for eleven NS-LMXBs (4U 1635–536, 4U 1705–44, 4U 1608–52, GS 1826–238, Aql X-1, XTE J1709–267, 4U 1820–30, M 15 X-2, Terzan 5 X-2, Terzan 5 X-3, and SAX J1748.9–2021). Among them, five sources (4U 1820–30, M 15 X-2, Terzan 5 X-2, Terzan 5 X-3, and SAX J1748.9–2021) are located in globular clusters. 4U 1820–30 is the only persistently bright source in the globular cluster, and contamination from other X-ray sources can be ignored. However, the other four sources are transients, whose quiescent states are affected by contamination. Therefore, it is difficult to estimate the average luminosity during quiescence. In M 15, although the outbursts was identified with M 15 X-2 (Tomida et al. 2013), X-ray emission in quiescence contains that of at least two X-ray sources, 4U 2127+11 and M 15 X-2 (White & Angelini 2001). In Terzan 5, two outbursts with clear spectral state transition were detected. The former outburst was identified with Terzan 5 X-2 (IGR J17480–2446: Ferrigno et al. 2010) and the latter was Terzan 5 X-3 (Swift J174805.3–244637: Wijnands et al. 2012). However, the quiescent flux was contributed by at least three sources: EXO 1745–248, Terzan 5 X-2, and Terzan 5 X-3 (Bahramian et al. 2014). The outburst of NGC 6440 was identified with SAX J1748.9–2021 (Suzuki et al. 2009). However, there are at least two sources SAX J1748.9–2021 and NGC 6440 X-2 (Heinke et al. 2010). Therefore, the four sources in globular clusters (M 15 X-2, Terzan 5 X-2, Terzan 5 X-3, and SAX J1748.9–2021) were excluded from further analysis in this paper. The properties of the seven investigated NS-LMXBs are summarized in table 1.

2.2. Threshold of state transition in the BAT/GSC hardness ratio

Figure 1 shows the histograms (number of days) of the BAT/GSC hardness ratios of the seven NS-LMXBs. Six of the NS-LMXB exhibit two peaks corresponding to the soft and hard states. The exception is 4U 1820–30, which exists almost exclusively in the soft state. Consequently, the dwell-time of the hard state is very short and its hard-

¹ <<http://maxi.riken.jp/>>.

² <<http://heasarc.gsfc.nasa.gov/docs/swift/results/transients/>>.

³ For 4U 1608–52, two values (3.6 and 4.1 kpc) were listed. In this paper, we employ 4.1 kpc according to Galloway et al. (2008). For GS 1826–238, the value of 4–8 kpc was listed, but we employ 7 kpc (Cocchi et al. 2011).

Table 1. Properties of the seven NS-LMXBs analyzed in this paper.

Name	State	P_{orbital} (hr)	Distance (kpc)	Reference*
4U 1636–536	Persistent	3.80	6	(1)
4U 1705–44	Persistent	unknown	7.4	(1)
4U 1608–52	Transient	12.89	4.1	(1), (2)
GS 1826–238	Persistent	2.088	7	(1), (3)
Aql X-1	Transient	18.95	5	(1)
XTE J1709–267	Transient	unknown	8.8	(1)
4U 1820–30	Persistent	0.19	7.6	(1)

* (1) Liu et al. 2007, (2) Galloway et al. 2008, and (3) Cocchi et al. 2011.

Table 2. Summary of spectral states for seven NS-LMXBs.

Name	Thresholds of hardness ratio*	Average $L_{2-10 \text{ keV}}$ †		Outburst type‡
		Hard state	Soft state	
4U 1636–536	0.253	2.94 ± 0.02	6.95 ± 0.02	mini
4U 1705–44§	0.355	4.22 ± 0.04	27.77 ± 0.04	normal
			7.22 ± 0.06	mini
4U 1608–52§	0.224	1.07 ± 0.01	11.43 ± 0.03	normal
			2.25 ± 0.05	mini
GS 1826–238	0.2	2.95 ± 0.01	8.15 ± 0.16	mini
Aql X-1	0.222	1.55 ± 0.02	23.6 ± 0.07	normal
4U 1820–30	0.2	17.61 ± 0.02	34.15 ± 0.03	other
XTE J1709–267	0.282	< 1.12	12.5 ± 0.1	normal

* Threshold between soft and hard states, which was determined using the distribution of the BAT/GSC hardness ratio in figure 1.

† Average luminosity in the 2–10 keV band in the unit of $10^{36} \text{ erg s}^{-1}$. The luminosity of hard and soft states are the averages of the bins in the left and right part of the vertical dotted line in figure 1, respectively.

‡ “normal” denotes that average luminosity of soft state is above $\sim 10^{37} \text{ erg s}^{-1}$ and “mini” denotes that that is below $\sim 10^{37} \text{ erg s}^{-1}$. For 4U 1820–30, we note “other” because average luminosity in both soft and hard state are above $\sim 10^{37} \text{ erg s}^{-1}$.

§ Those sources had two types of soft states with clearly different luminosities.

state peak is unclear. We basically adopted the luminosity of the lowest point between the two peaks as the threshold between the soft and hard states. When the lowest points were unclear (Aql X-1), we adopted the center value of the right end of the soft-state distribution and the left end of the hard-state distribution. The threshold of 4U 1820–30 was determined at the right end of the Gaussian distribution of the soft state, where excess points first appear.

The thresholds between the soft and hard states are summarized in table 2. Figures 2 and 3 show the GSC light curves, BAT light curves, and hardness ratios (BAT/GSC) of the seven sources. In these figures, the thresholds separate the data points into soft and hard states.

2.3. Mini-outburst and normal outburst

We calculated the average 2–10 keV luminosities of the soft and hard states using the thresholds of the hardness ratios in table 2. Here, the hard state of XTE J1709–267 was obscured by the detection limit of this source ($\sim 10^{36} \text{ erg s}^{-1}$). Thus, the calculated average luminosity in the hard state corresponds to the upper limit. Two types of soft states with different luminosities were noticed in

4U 1705–44 and 4U 1608–52. The luminosities differ by factors of 3–5 despite being in the soft state. In 4U 1705–44, the soft-state luminosities were lower during MJD = 55058–55400 and 55800–56100 than during other soft-state parts. Therefore, we calculated the average luminosity of each soft state. 4U 1608–52 exhibited a low-luminosity soft state (below $5 \times 10^{36} \text{ erg s}^{-1}$) during MJD = 55900–56100. Thus, the average luminosity during MJD = 55900–56100 was separately calculated in table 2. The luminosity dwell-time distributions of 4U 1705–44 and 4U 1608–52 also exhibit two soft states with different luminosities (see figure 4).

In table 2, the soft states of all sources are separated into two luminosity classes. If the average luminosity in the soft state is below $\sim 10^{37} \text{ erg s}^{-1}$, the X-ray variability (repeated small increase) is called “mini-outbursts,” whereas outburst with average luminosity above $\sim 10^{37} \text{ erg s}^{-1}$ is called “normal outburst.” For 4U 1820–30, the average luminosities of both soft and hard states are above $\sim 10^{37} \text{ erg s}^{-1}$. This source remains in the soft state unless the luminosity in the 2–10 keV band decreased below $\sim 3 \times 10^{37} \text{ erg s}^{-1}$. The hard states were identified around MJD ~ 55294 , 55622, 56135, and 56990. The X-ray vari-

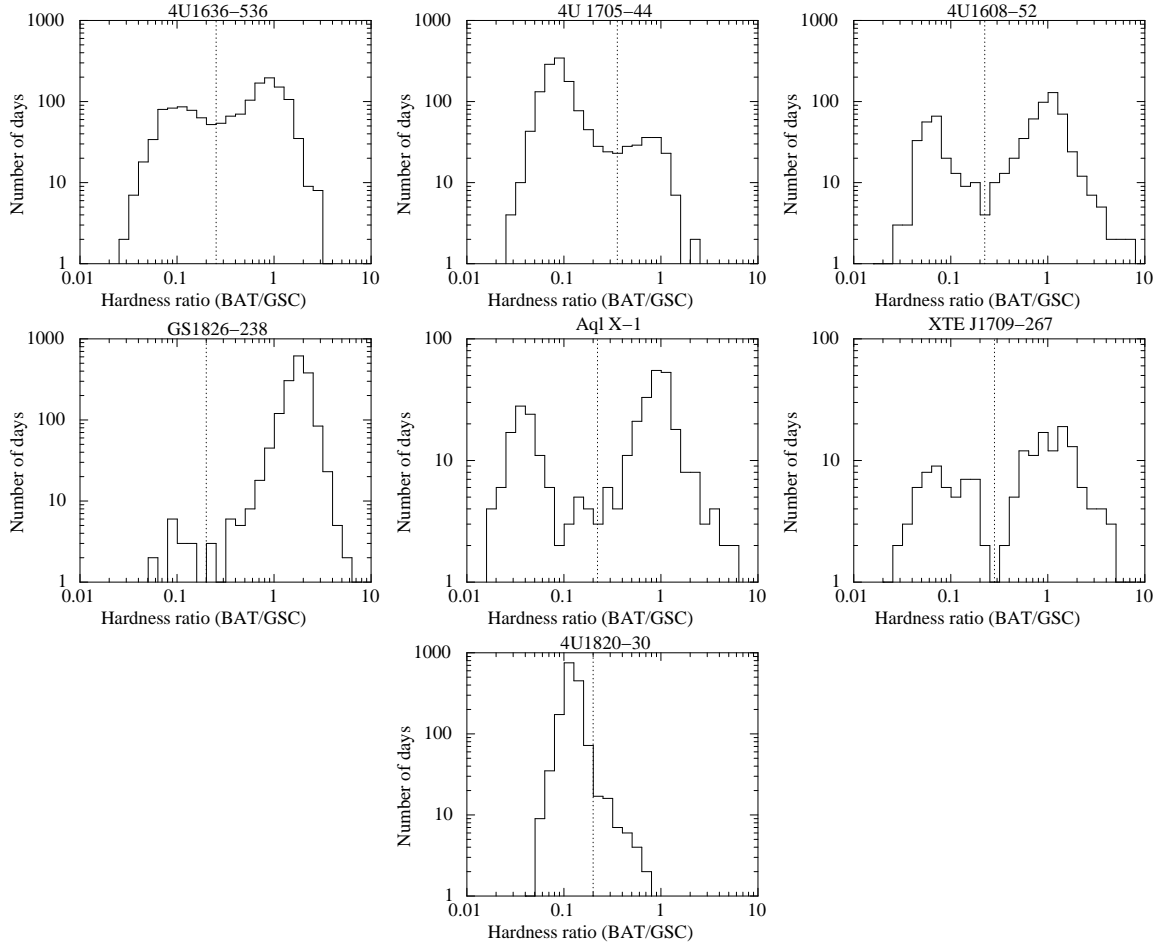


Fig. 1. Distributions of hardness ratios of BAT/GSC for seven NS-LMXBs. Distributions were constructed from data with a significance $> 1 \sigma$. The vertical dotted lines represented the threshold between soft and hard states (see text for explanation).

ability cannot be described as an outburst. Therefore, we categorized it as the “other,” signifying a different phenomenon.

Figure 5 shows typical mini-outburst from 4U 1636–536, 4U 1705–44, 4U 1608–52, and GS 1826–238. These plot are magnified regions of their corresponding light curves in figure 2. The individual properties of mini-outburst in the four sources are summarized as follows:

4U 1636–536: Mini-outburst occurred repeatedly with a period of ~ 30 –50 d while the X-ray luminosity gradually declined (from $\sim 6 \times 10^{36}$ to $\sim 3 \times 10^{36}$ erg s $^{-1}$ in the 2–10 keV band). Similar behaviour has been observed since 2002 (Shih et al. 2005, 2011; Belloni et al. 2007; Lyu et al. 2014).

4U 1705–44: Mini-outburst occurred repeatedly during the periods of no normal outbursts. The mini-outbursts had shorter durations than normal outbursts (see figure 2). The spectral state transition during the periods of no normal outbursts has been also reported by Homan et al. (2009) and Lin, Remillard, and Homan (2010).

4U 1608–52: Four mini-outbursts were identified on MJD = 55994, 56031, 56046, and 56749 (dates of

peak luminosity; see also figure 5). The four mini-outbursts occurred at the last period of long hard state after normal outburst, where the hard-high state is determined by Matsuoka and Asai (2013).

GS 1826–238: Mini-outburst occurred while the X-ray luminosity gradually increased (from $\sim 2 \times 10^{36}$ to $\sim 5 \times 10^{36}$ erg s $^{-1}$ in the 2–10 keV band). Although the luminosity in 2–10 keV band increased by only a few times in the mini-outburst, the luminosity in the 15–50 keV band decreased by about one order of magnitude. Therefore, the spectral state transition was clear. The spectral state transition has been already reported by Nakahira et al. (2014).

2.4. Determination of transition luminosity

We examine the luminosities of hard-to-soft and soft-to-hard transitions. Here, we adopt the luminosity in the 2–10 keV band, because the radiation in this band is dominant in bright NS-LMXBs. First, we divided the data bins into two states (soft or hard), using the thresholds of hardness ratio in table 2. A hard-to-soft transition is defined as a soft state continues for over two days after a hard state and vice versa, using the data with a significance of

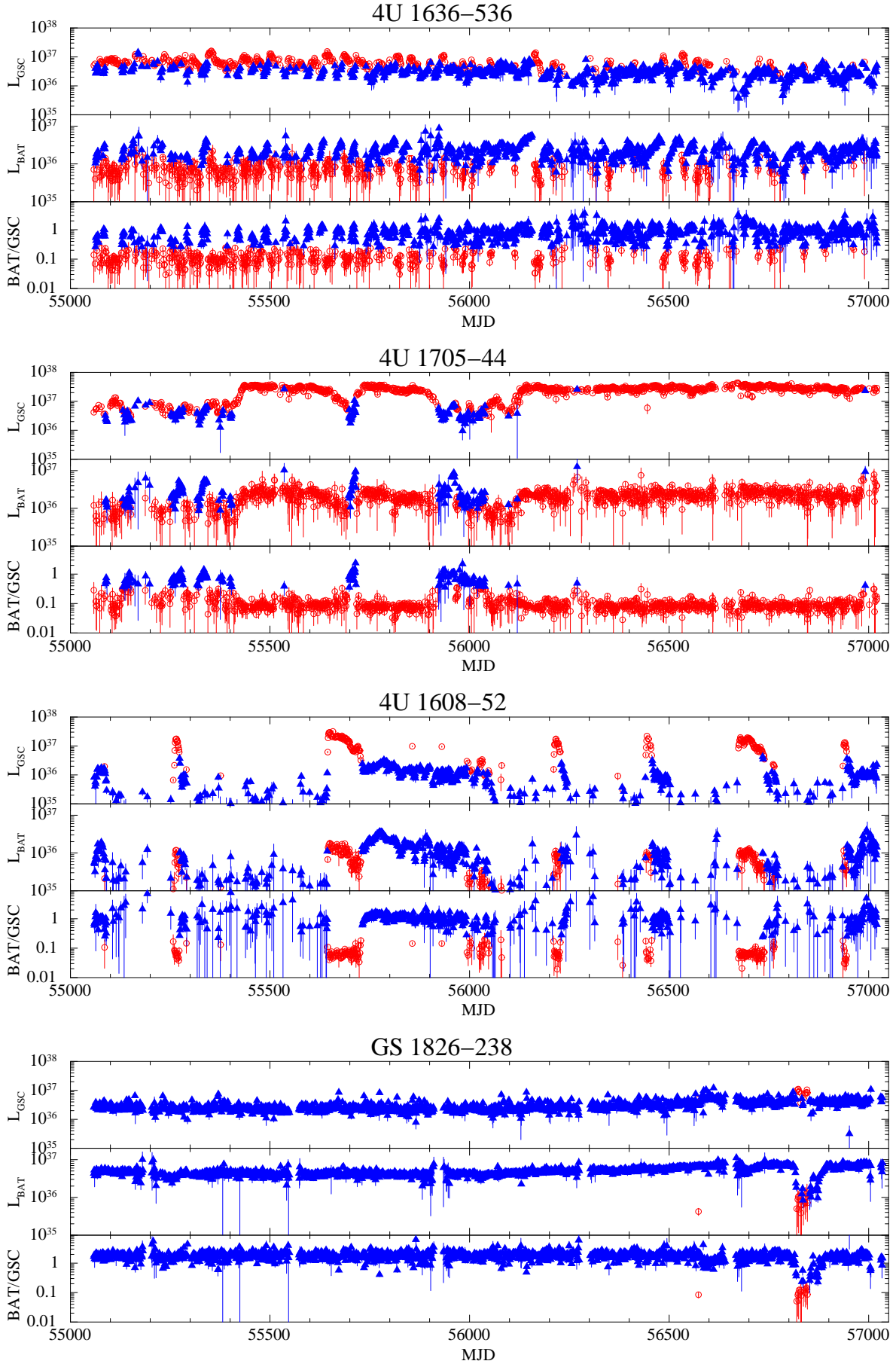


Fig. 2. One-day GSC light curves in the 2–10 keV band, one-day BAT light curves in the 15–50 keV band, and the hardness ratio (BAT/GSC) of 4U 1636–536, 4U 1705–44, 4U 1608–52, and GS 1826–238. L_{GSC} and L_{BAT} are the luminosities in units of erg s^{-1} . Vertical error bars represent $1-\sigma$ statistical uncertainty. Red circles and blue triangles represent data of soft and hard states,

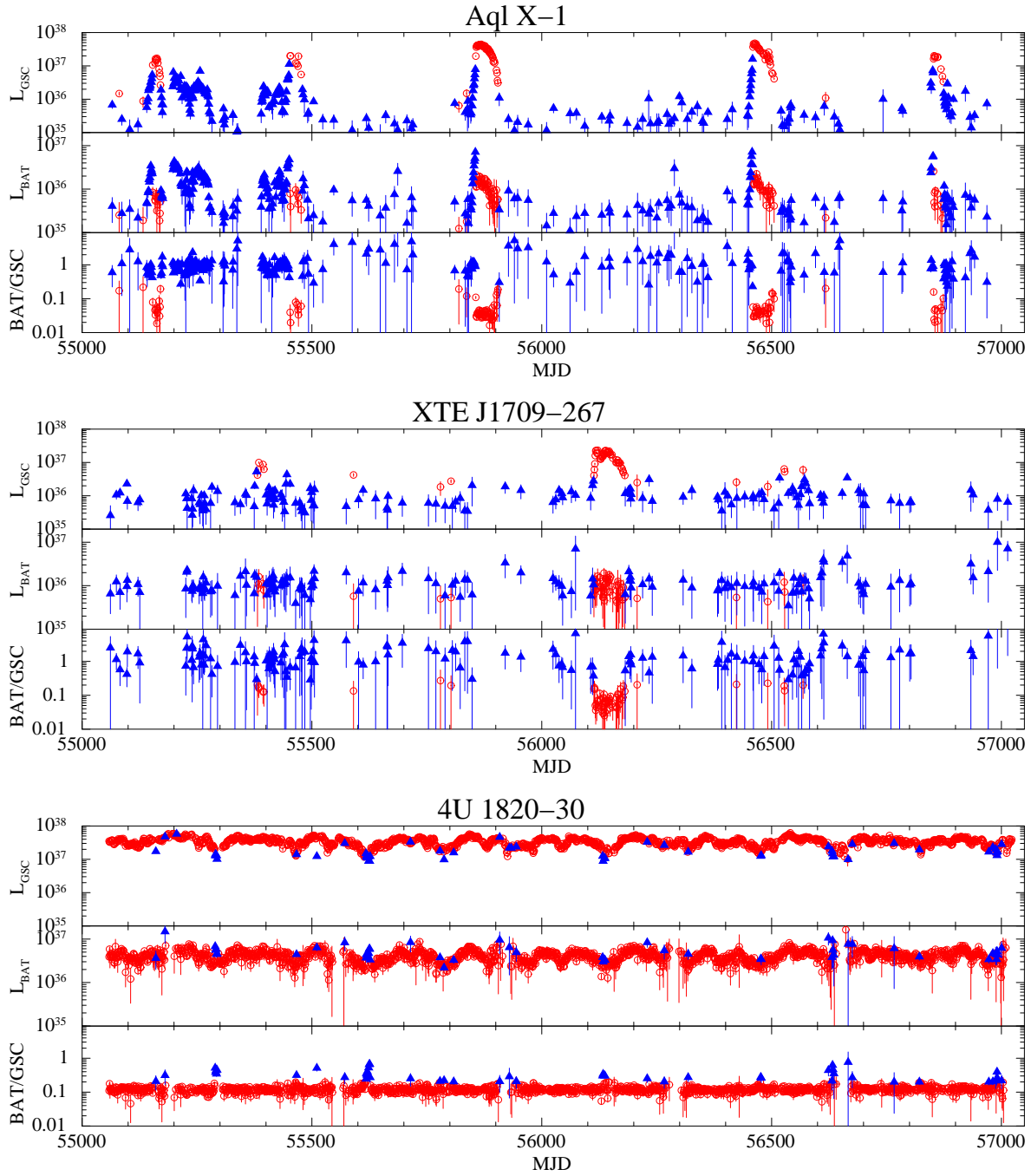


Fig. 3. Same as figure 2, but for Aql X-1, XTE J1709-267, and 4U 1820-30. (Color online)

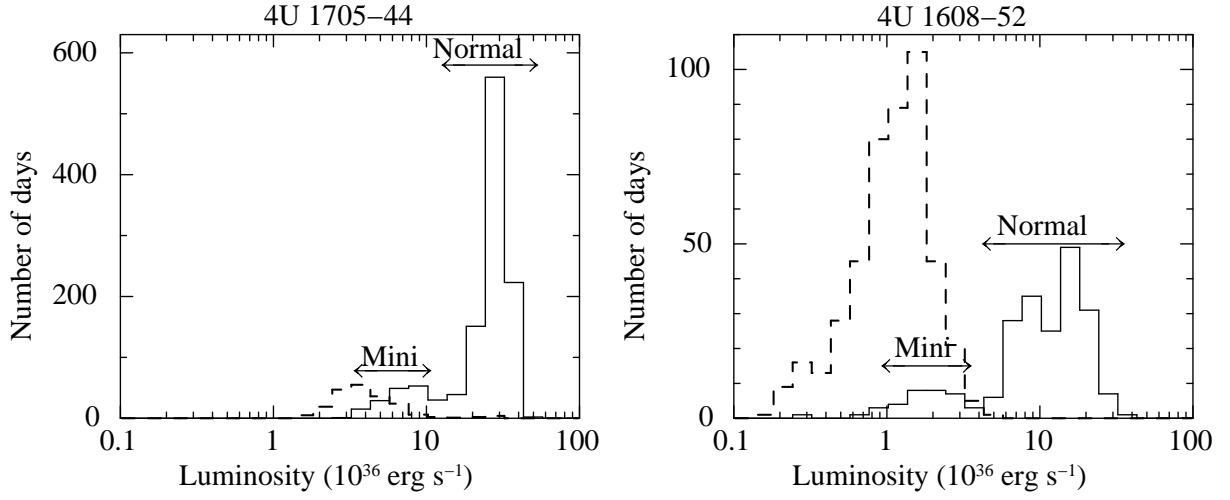


Fig. 4. Luminosity dwell-time distributions of 4U 1705–44 and 4U 1608–52. The solid- and dashed-line histograms show the data of soft and hard states, respectively. We identified two types of soft states with different luminosities. Horizontal arrows indicate the ranges of soft states in mini-outbursts and normal outbursts.

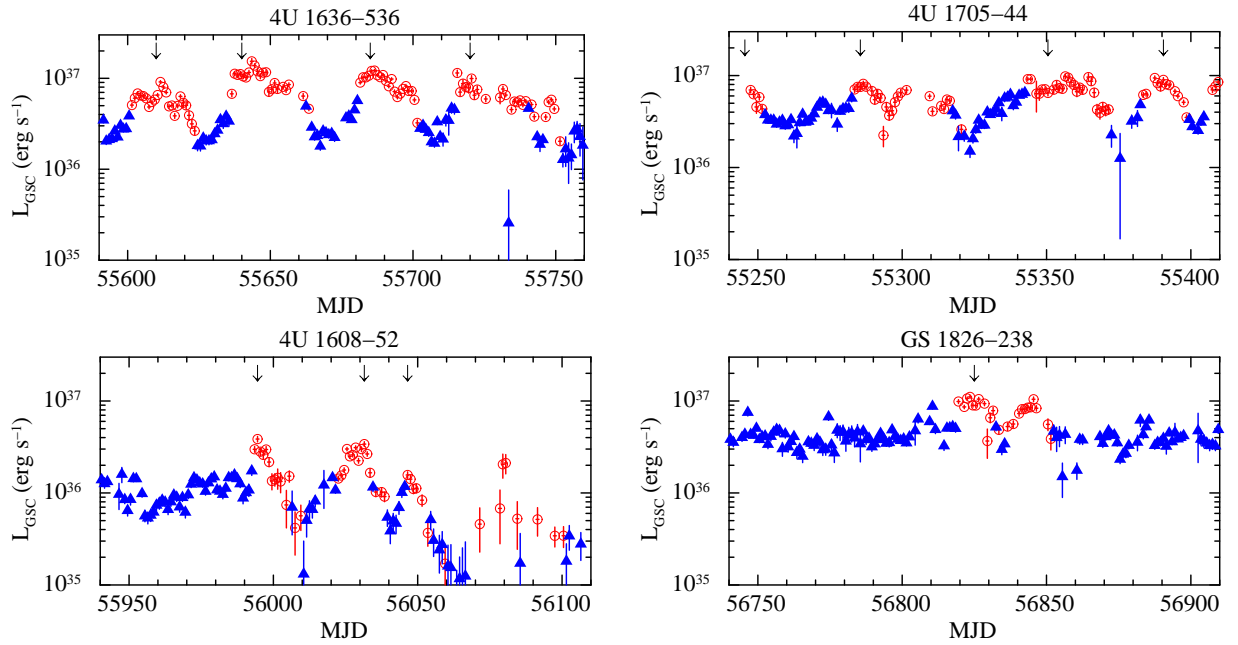


Fig. 5. Magnified light curves of 4U 1636–536, 4U 1705–44, 4U 1608–52, and GS 1826–238. Mini-outbursts are indicated by arrows. Red circles and blue triangles represent data of soft and hard states, respectively. (Color online)

more than 1σ . The time and luminosity of the hard-to-soft transition is estimated by the “last hard-state” bin and the “first soft-state” bin using the method described in Asai et al. (2012). We employ the center of the two data bins as “transition time (the time when transition occurs)” and their time interval as the error on it. We also define the average luminosity in this time interval as the “transition luminosity.” The soft-to-hard transition is similarly defined. Figure 6 plots the hard-to-soft and soft-to-hard transition luminosities of the seven LMXBs. In this figure, the data points of “mini” and “other” (as defined in table 2) are plotted by “filled circles,” and are distinguished from the data of normal outburst (open circles). All transition luminosities of 4U 1820–30 categorized as “other” are higher than 10^{37} erg s $^{-1}$, which is clearly higher than 4% of L_E even after spectral and bolometric correction as described in subsection 2.1. We discuss such high transition luminosities in subsection 3.1.

Most of transition luminosities of 4U 1636–536 for both hard-to-soft and soft-to-hard transitions are in the range of $(2\text{--}10)\times 10^{36}$ erg s $^{-1}$. The transition luminosity would be independent of the luminosity before the transition. This behaviour was also confirmed in figure 7. Here, we divided the observation period into two periods (MJD = 55058–56000 and MJD = 56000–56899) and plotted the luminosity dwell-time distribution during each period. The average luminosities of the earlier and later periods were $(5.56 \pm 0.01) \times 10^{36}$ erg s $^{-1}$ and $(3.3 \pm 0.02) \times 10^{36}$ erg s $^{-1}$, respectively. As the luminosity declined, the dwell-time of the soft state became shorter, whereas that of the hard state became longer. This means that the transition luminosity remains almost constant.

In five normal outbursts (2011-Jun of 4U 1705–44, 2010-Sep, 2011-Oct, 2013-Jun, and 2014-Jul of Aql X-1), the hard-to-soft transition luminosities are higher than 10^{37} erg s $^{-1}$, which is higher than 4% of L_E . These outbursts with higher hard-to-soft transition luminosities are classified as S-type defined by Asai et al. (2012).

In a normal outburst of 4U1608–52 (2010-Mar), the hard-to-soft transition luminosities are lower than 10^{36} erg s $^{-1}$, which would be 1% of L_E . However, the data bins of the first soft state in the one-day BAT light curve have relatively large uncertainties. For example, at a significance level exceeding 2σ , no data bins can be assigned to the first soft state, because of large data gaps. The lowness of the transition luminosity depends on the data quality, so is not discussed here. The time and luminosity of the state transitions and the soft-state durations of normal outbursts from 4U 1705–44, 4U 1608–52, Aql X-1, and XTE J1709–267 are summarized in table 3.

3. Discussion

3.1. Transition luminosity

We investigated the luminosities in the 2–10 keV band of hard-to-soft and soft-to-hard transitions in seven sources. There are two cases in which the transition luminosities are higher than 10^{37} erg s $^{-1}$, which is higher than 4% of L_E . The one is the luminosities of S-type hard-to-

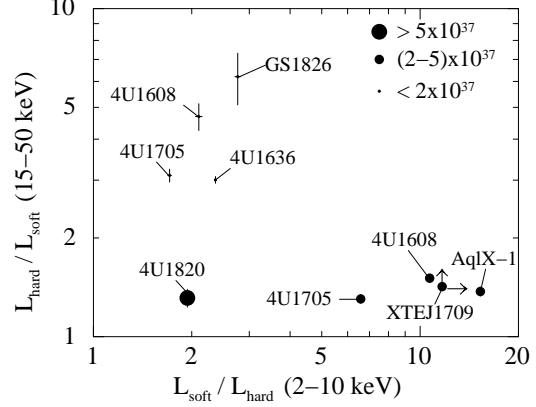


Fig. 8. Average luminosity ratios of the soft and hard states in the 2–10 keV band (GSC) and the 15–50 keV band (BAT). Mark size represents the peak luminosity of the soft state. The data point of XTE J1709–26 is a lower limit because of the detection limit during the period of no outbursts.

soft transitions (Asai et al. 2012), which are higher than 4% of L_E . According to Asai et al. (2012), X-ray irradiation before the outbursts might heat up the accretion disk and delay the optically thin-to-thick disk transition. In this scenario, the optically thin-to-thick disk transition would be suppressed by the large Compton cloud formed by the X-ray irradiation. The S-type outbursts identified in this study were five normal outbursts from 4U 1705–44 and Aql X-1.

The other is the transition luminosities of 4U 1820–30. Such high transition luminosities are similar to the hard-to-soft transitions of S-type in normal outburst. Both soft and hard states exhibited high average luminosity in the 15–50 keV band [soft state: $(4.07 \pm 0.02) \times 10^{36}$ erg s $^{-1}$, hard state: $(5.3 \pm 0.3) \times 10^{36}$ erg s $^{-1}$]. It is suggested that the Compton cloud is large and an optically thin disk could exist at such high luminosity. Titarchuk et al. (2013) analyzed the RXTE data of 4U 1820–30 over a similar epoch of luminosity decrease to our data analysis. They reported that a dramatic rise in the electron temperature of the Compton cloud (from 2.9 to 21 keV) and a state transition from upper banana to island. The results support that the optically thick-to-thin disk transition occurs at such high luminosity.

In summary, the spectral state transition usually corresponds to the state transition of the inner accretion disk. However, spectral state transition might result from changes in not only the disk state but also the electron temperature of the Compton cloud.

3.2. Properties of mini-outburst

As described in subsection 2.3, the X-ray variability with spectral state transition was divided into mini-outburst and normal outburst by the average luminosity of the soft state in the 2–10 keV band. Moreover, in the 15–50 keV band, the ratio of the average luminosities in the soft and hard states also differed between mini-outbursts and normal outbursts. Figure 8 shows the ratios of the average luminosities of the soft and hard states in the

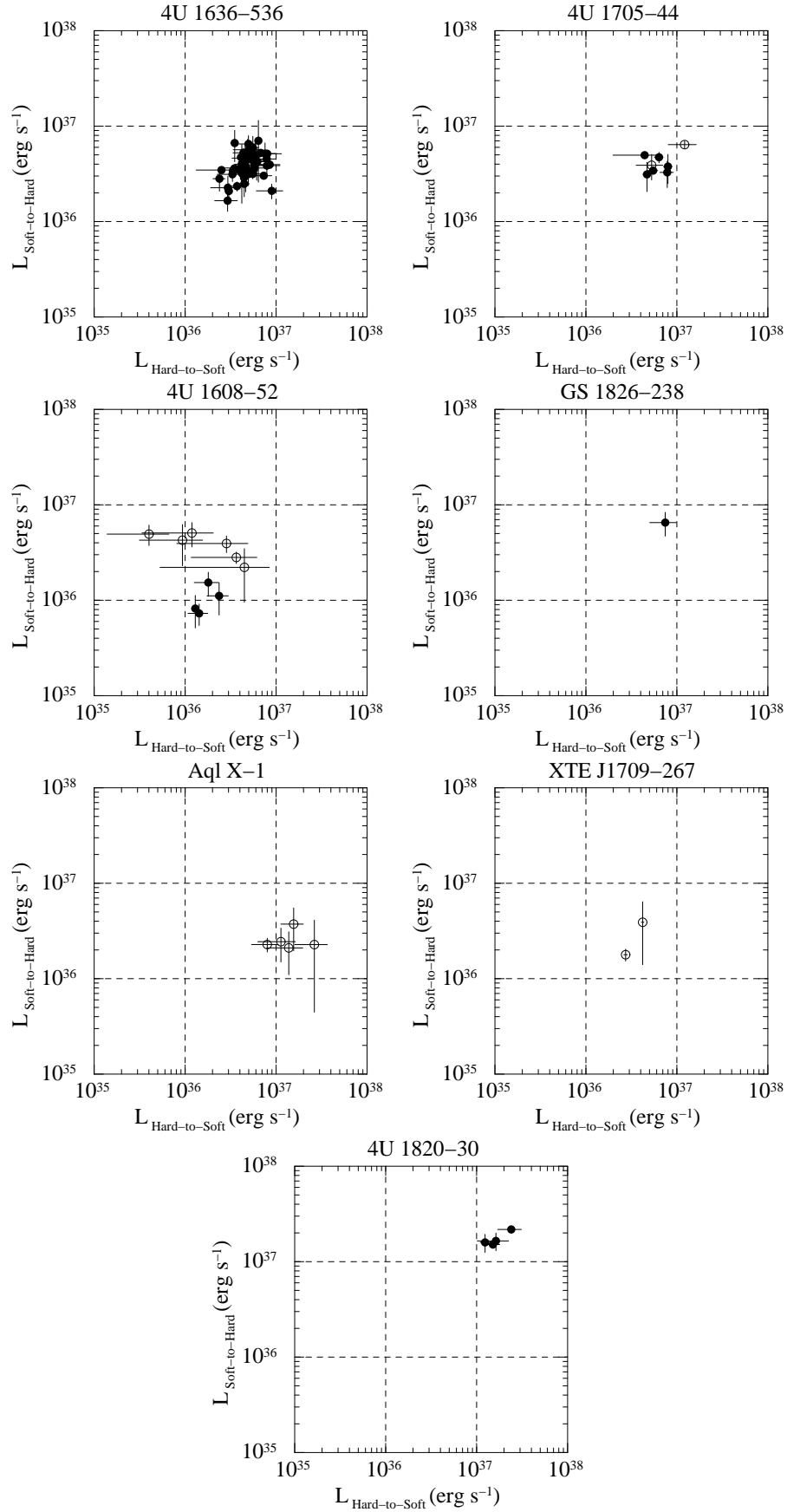


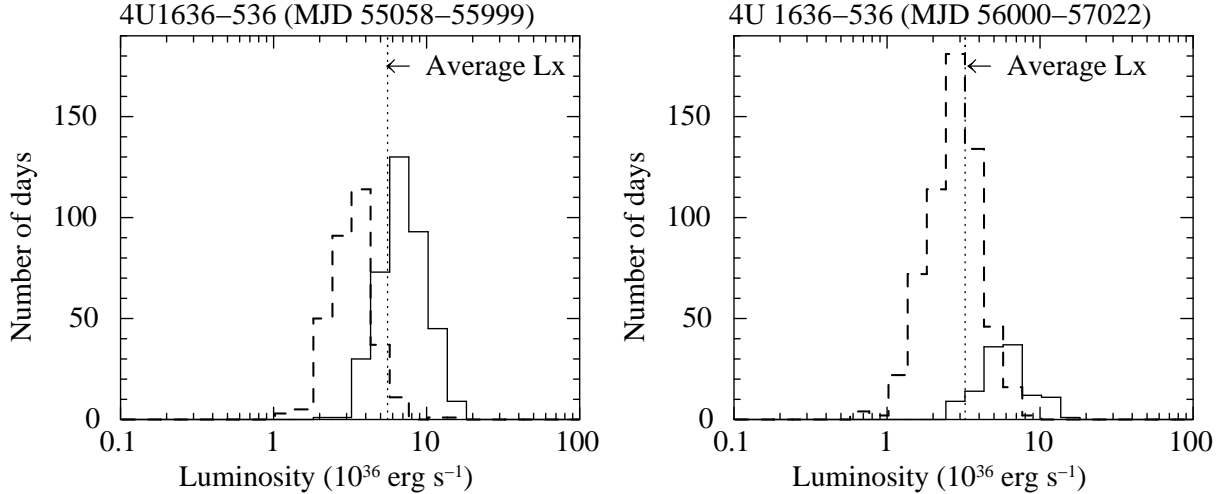
Fig. 6. Transition luminosity (2-10 keV) of hard-to-soft and soft-to-hard transitions. Transitions in normal outburst are marked by open circles, and others (“mini” and “other” in table2) are marked by filled circles.

Table 3. Summary of normal outbursts from 4U 1705–44, 4U 1608–52, Aql X-1, and XTE J1709–267

Normal outburst	Hard-to-soft transition		Soft-to-hard transition		Duration of soft state (d)
	Time (MJD)	Luminosity*	Time (MJD)	Luminosity*	
4U 1705–44					
2010-Jul	55406.0 ± 1.5	5.3 ± 1.7	55695.5 ± 2.0	4.0 ± 1.1	289.5 ± 3.5
2011-Jun	55716.0 ± 0.5	12.2 ± 4.1	55921.5 ± 1.0	6.4 ± 0.6	205.5 ± 1.5
2012-Apr	56039.0 ± 0.5	6.6 ± 0.3	–†	–†	–†
4U 1608–52					
2010-Mar	55254.5 ± 3.0	0.4 ± 0.3	55273.0 ± 0.5	4.9 ± 1.2	18.5 ± 3.5
2011-Mar	55644.0 ± 0.5	3.7 ± 2.5	55729.5 ± 2.0	2.8 ± 0.4	85.5 ± 2.5
2012-Oct	56209.0 ± 1.5	0.9 ± 0.6	56228.5 ± 1.0	4.3 ± 2.0	19.5 ± 2.5
2013-May	56441.0 ± 0.5	2.8 ± 2.0	56457.0 ± 0.5	3.9 ± 0.8	16.0 ± 1.0
2014-Jan	56672.0 ± 1.5	4.5 ± 4.0	56741.5 ± 3.0	2.2 ± 1.3	69.5 ± 4.5
2014-Oct	56935.0 ± 0.5	1.2 ± 9.0	56945.0 ± 0.5	5.1 ± 1.1	10.0 ± 1.0
Aql X-1					
2009-Nov	55153.0 ± 0.5	8.0 ± 3.0	55171.0 ± 0.5	2.3 ± 0.4	18.0 ± 1.0
2010-Sep	55451.5 ± 1.0	15.6 ± 4.3	55478.0 ± 1.5	3.7 ± 1.8	26.5 ± 2.5
2011-Oct	55856.0 ± 0.5	13.8 ± 5.9	55906.0 ± 1.5	2.1 ± 1.0	50.0 ± 2.0
2013-Jun	56459.0 ± 0.5	26.3 ± 10.3	56513.0 ± 7.5	2.3 ± 1.8	54.0 ± 8.0
2014-Jul	56582.0 ± 0.5	11.3 ± 5.0	56874.0 ± 0.5	2.4 ± 0.9	22.0 ± 1.0
XTE J1709–267					
2010-Jul	55380.5 ± 1.0	4.8 ± 0.6	55398.0 ± 2.5	3.7 ± 2.6	17.5 ± 3.5
2012-Aug	56113.0 ± 0.5	3.4 ± 0.6	56181.0 ± 0.5	2.6 ± 1.5	68 ± 1

* Luminosity in the 2–10 keV band in the unit of 10^{36} erg s $^{-1}$.

† The outburst was continuing at the end of this observation (2015.12.31)

**Fig. 7.** Luminosity dwell-time distributions of 4U 1636–536. The distributions were constructed from the data with a significance of more than 3σ . Left-hand panel displays the distributions of the data for MJD 55058–55999. Right-hand panel is the data for MJD 56000–57022. Solid- and dashed line histograms were constructed from data of soft and hard states, respectively. The vertical dotted lines indicate the average luminosity during each period.

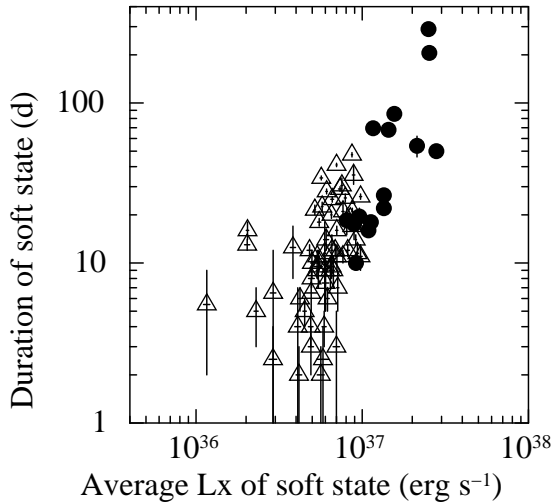


Fig. 9. Duration vs. average luminosity of the soft states in the 2–10 keV band. Filled circles and open triangles represent data of normal outbursts and mini-outbursts, respectively. The data of 4U 1820–30 were excluded from this figure, because the behaviour is different from that of both normal outburst and mini-outburst as described in table 2 and subsection 2.3.

2–10 keV band and that in the 15–50 keV band. The ratio in the 15–50 keV band is larger in the mini-outbursts than in normal outbursts. The difference is relevant to the duration of the soft state. Figure 9 plots the duration versus the average luminosity of the soft states. Here, we excluded the data of 4U 1820–30, which behave differently from both normal outburst and mini-outburst as described in table 2 and subsection 2.3. The mini-outbursts tend to have shorter durations than normal outbursts. In both mini-outburst and normal outburst, the luminosity in the 15–50 keV band drops once at the hard-to-soft transition, then increases again. The post-transition increase is caused by the increase of seed photons (see figure 8 in Asai et al. 2012). However, in the short duration of mini-outburst, the 15–50 keV luminosity does not recover to its hard-state level just before the transition. Therefore, the luminosity ratio of the soft and hard states becomes large in the 15–50 keV band.

The properties of mini-outburst are summarized as follows: (1) mini-outburst has smaller amplitude and shorter duration than those of normal outburst, and (2) most of the transition luminosities of mini-outbursts are in the range of 1%–4% of L_E . Therefore, both mini-outburst and normal outburst would be similarly interpreted by the disk instability model. The time scale of the mini-outburst supports the disk instability model. Following Frank, King, and Raine (1992), we estimated the viscous time scale in the outer disk. The viscous time scale was given by

$$t_{\text{visc}} \sim 3 \times 10^5 \alpha^{-4/5} \dot{M}_{16}^{-3/10} M_{\text{NS}}^{1/4} (R_d/10^{10})^{5/4} \text{ s}, \quad (1)$$

where \dot{M}_{16} is the mass accretion rate in units of 10^{16} g s^{-1} , M_{NS} is the neutron star mass of $1.4M_\odot$, and R_d is the outer radius of the accretion disk. Assuming that α

$= 0.1$ – 1 , $\dot{M}_{16} = 5.3$ ($L_x \sim 10^{37} \text{ erg s}^{-1}$, the maximum luminosity of a mini-outburst), and $R_d \sim 3 \times 10^{10} \text{ cm}$ (the R_d of 4U 1636–536; see figure 9 in the next subsection), we obtained $t_{\text{visc}} \sim 10$ – 60 d . This time scale is roughly comparable with the typical time scale of a mini-outburst. Furthermore, Mineshige and Osaki (1985) predicted a small-amplitude variability (resembling a mini-outburst) in the disk instability model, although their calculation assumed a dwarf nova. We discuss the relation of the mini-outburst and the disk instability model in the next subsection.

The periodic variability observed in KS 1731–320 is similar to the mini-outbursts in 4U 1636–536, although the presence of spectral state transitions is unclear. According to Revnivtsev and Sunyaev (2003), KS 1731–320 exhibited strong variability on a monthly time scale during MJD ~ 51100 – 52000 . They interpreted the periodic variability as disk precession. The luminosity in the 2–10 keV band obtained from the public data of ASM on RXTE, was between $\sim 3 \times 10^{36} \text{ erg s}^{-1}$ and $\sim 1 \times 10^{37} \text{ erg s}^{-1}$, assuming a distance of 7 kpc (Muno et al. 2000). The luminosity range of the variability is close to 1%–4% of L_E . Therefore, we suggest that the variability could result from a repeat of mini-outburst.

Simon (2010) referred the variability in KS 1731–320 that follows the main outburst as “echo outbursts.” They suggested that echo outbursts are triggered by the configuration of the inner ionized stable region surrounded by the outer unstable region. They also pointed out the important role of thermal instability of the accretion disk in the luminosity decline. Shih et al. (2005) also reported that the variability during the X-ray decline in both 4U 1636–536 and KS 1731–260 was similar. They suggested the relation of the variability and the thermal instability of an accretion disk.

3.3. Mini-outburst and disk instability model

Normal outbursts in NS-LMXBs are usually interpreted by the disk instability model like the outburst of dwarf novae. The theoretical disk instability model of Mineshige and Osaki (1983, 1985) predicts both large-amplitude outbursts (roar type) and small-amplitude variability (purr type). The former is considered to correspond to normal outburst, but no correspondence has been found for the latter. Here, we propose that purr-type outbursts correspond to mini-outbursts, because the characteristics (small-amplitude and short duration) of both types are quite similar.

We now discuss the possibility of the purr-type outburst. Most of the transition luminosities of mini-outbursts were in the range of 1%–4% of L_E . It would indicate that the spectral state transitions are due to the inner disk transitions, which are caused by thermal instability of the outer disk. The main difference of the two-types instability (roar type and purr type) is in the assignment of α parameter. The α parameter is usually considered to depend on the disk temperature, although there are several theoretical models (e.g., Hameury et al. 1998). In order to explain a normal outburst, a high α is

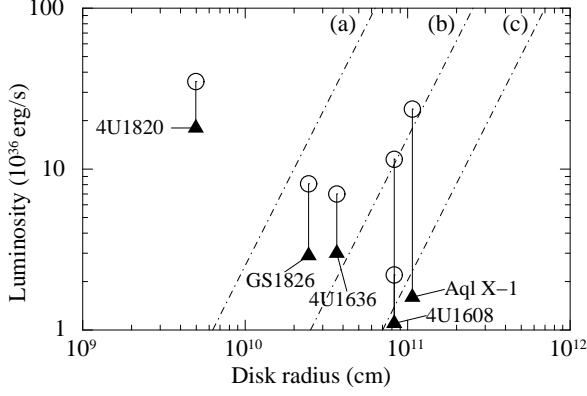


Fig. 10. Average X-ray luminosity in the 2–10 keV band as a function of outer disk radius. Open circles and filled triangles represent data of soft and hard states, respectively. Theoretical lines of (a), (b), and (c) are calculated by equation (2) with $C = 10^{-4}$ (Tuchman et al. 1990). The irradiation temperatures of (a), (b), and (c) are $T_{\text{irr}} = 10000$ K, 5000 K, and 3000 K, respectively.

assigned in a hot state (upper branch in S-shape curve) and a low α is assigned in a cool state (lower branch). As a result, the S-shape curve is modified and the width of the middle branch is extended. This means that the instability can propagate through the whole disk (roar type). On the other hand, when the same α is assigned in both a hot and cool state (upper and lower branch), the width of the middle branch is narrow, and then the instability cannot propagate through the whole disk (purr type).

Here, we examine the influence of the irradiation on the S-shaped curve. Tuchman, Mineshige, and Wheeler (1990) calculated the instability under irradiation and generated the S-shaped curves at different irradiation temperatures (see figure 1 in Tuchman et al. 1990). There are two modifications of the S-shaped curve due to the irradiation. One is to move the lower branch upward in the diagram and the other is to shorten the width of the middle branch. Those two lead to that the α -value of the lower branch becomes close to that of the upper branch, and then the approximation of a constant- α disk would be suitable.

Next, we investigate status of the outer disk (stable or unstable) assuming that the disk temperature is determined by X-ray heating. Figure 10 shows the average X-ray luminosity of the soft (open circles) and hard (filled triangles) states in the 2–10 keV band as a function of the outer radius of the accretion disk. Here, the outer radius was assumed as 0.35 of the binary separation (Smak 1982). The binary separation was estimated by Kepler’s third law assuming a neutron star mass of $1.4 M_{\odot}$. The orbital periods were taken from the LMXB catalogue (Liu et al. 2007) and are listed in table 1. The mass of the companion star was taken as $0.4 M_{\odot}$ although the actual mass is uncertain. 4U 1705–44 and XTE J1709–267 were excluded from this analysis because their orbital periods are not known.

The theoretical lines of (a), (b), and (c) indicate the

“irradiation disk temperatures” which depended on X-ray heating and was calculated by equation (53) of Tuchman et al. (1990). The equation (53) was expressed as

$$T_{\text{irr}} \simeq 10^{3.9}(\text{K}) \left(\frac{C}{10^{-4}} \right)^{1/4} \left(\frac{L}{10^{37} \text{ erg s}^{-1}} \right)^{1/4} \left(\frac{R_d}{10^{10.5} \text{ cm}} \right)^{-1/2} \quad (2)$$

Here, T_{irr} is called the “irradiation disk temperature,” defined by the irradiation flux as $F_{\text{irr}} = \sigma T_{\text{irr}}^4$. F_{irr} is the irradiation flux on the disk surface from external heat sources. The thermal unstable branch (the middle branch of the S-shaped curve) disappears for strong irradiation with $T_{\text{irr}} \geq 10000$ K. The parameter C denotes the fraction of external heat caught by the outer disk. L is the X-ray luminosity of the external heat source and R_d is outer radius of accretion disk. Mineshige, Tuchman, and Wheeler (1990b) reported that if the irradiation is a function of the mass accretion rate and is not so strong ($C \sim 10^{-4}$ and $T_{\text{irr}} \leq 5000$ K), the model can reproduce the observed light variations of dwarf novae and it is relevant to the outburst of soft X-ray transients with large amplitudes (roar type).

Thus, we adopted $C = 10^{-4}$ and drew the three theoretical lines of (a), (b), and (c). The irradiation temperatures of (a), (b), and (c) are $T_{\text{irr}} = 10000$ K, 5000 K, and 3000 K, respectively. The line of (a) separates the stable and unstable regions. The left side of the line of (a) indicates the stable region (fully ionized region). The region between line (a) and (b) indicate the unstable region where the normal outburst (roar type) would not occur although the borderline depends on the model parameter such as C . Thus, in the region between (a) and (b), a constant- α disk would be applicable and then the purr-type instability would occur. In other words, the observed mini-outbursts are interpreted as the instability of the purr type in this region.

In figure 10, except for 4U 1820–30, all four sources have the unstable region between (a) and (b). It is consistent with the results that mini-outbursts (purr type) were observed in 4U 1636–536, GS 1826–238, and 4U 1608–52. However, in Aql X-1, the mini-outbursts were not observed in our observations. We suggest that it is relevant to the short period of hard-high state defined by Matsuoka and Asai (2013). For both 4U 1636–536 and GS 1826–238 (persistent sources), the outer radii at the hard-state luminosity locate on the left side of (b), which means the normal outburst (roar type) would not occur at these luminosities. It is consistent with the results that normal outbursts have not been observed in both sources. On the other hand, for both 4U 1608–52 and Aql X-1 (transient sources), the outer radius at the hard-state luminosity locate on the right side of (b), where the normal outburst (roar type) would occur. It supports that the normal outburst in NS-LMXB is caused by disk instability in the same way of dwarf novae, which has been pointed out by van Paradijs (1996).

Variability lasting several tens of days, which are often observed in the hard state of NS-LMXBs, might result from a repeat of mini-outburst although they do not accompany spectral state transitions. Such variability was

observed in both 4U 1608–52 and 4U 1636–536. In 4U 1608–52, variabilities without spectral state transitions were observed during MJD = 56700–56100 (hard-high state). In 4U 1636–536, variabilities in the period after MJD \sim 56000 do not always accompany spectral state transition. Because the maximum luminosity of the variability was below the transition luminosity, inner disk state transition would not occur.

4. Conclusion

We investigated the spectral state transitions in bright NS-LMXBs using the one-day bin light curves of MAXI/GSC and Swift/BAT. In four of the sources (4U 1636–536, GS 1826–238, 4U 1705–44, and 4U 1608–52), we detected small-amplitude X-ray variabilities with spectral state transitions. We named these variabilities “mini-outbursts” and interpreted them as disk instability based on a constant- α disk by Mineshige and Osaki (1985). In the case of mini-outburst, the S-shaped curves in the surface density and mass accretion rate diagram, are modified by the irradiation, and then the approximation of a constant- α disk would be suitable. Here, we call mini-outburst as “purr-type outburst” referring to theoretical studies by Mineshige and Shields (1990a).

We also suggest that variabilities in the hard state may be a repeat of mini-outbursts even if spectral state transitions do not occur. In this case, the state transition of an inner disk would not occur because the maximum luminosity of the variability is below the transition luminosity.

We would like to acknowledge Prof. S. Mineshige for the useful comment and discussion on this work. We also would like to acknowledge the MAXI team for MAXI operation and for analyzing real-time data. This research was partially supported by JSPS KAKENHI Grant Number 15H00288. This research was partially supported by the Ministry of Education, Culture, Sports, Science and Technology (MEXT), Grant-in-Aid for Science Research (24340041).

References

- Altamirano, D., Casella, P., Patruno, A., Wijnands, R., & van der Klis, M. 2008, *ApJ*, 674, L45
- Asai, K., et al. 2012, *PASJ*, 64, 128
- Bahramian, A., et al. 2014, *ApJ*, 780, 127
- Barthelmy, S. D., et al. 2005, *Space Sci. Rev.*, 120, 143
- Belloni, T., Homan, J., Motta, S., Ratti, E., & Méndez, M. 2007, *MNRAS*, 379, 247
- Cocchi, M., Farinelli, R., & Paizis, A. 2011, *A&A*, 529, A155
- de Jong, J. A., van Paradijs, J., & Augusteijn, T. 1996, *A&A*, 314, 484
- Done, C., Gierliński, M., & Kubota, A. 2007, *A&A Rev.*, 15, 1
- Ferrigno, C., Brandt, S., Kuulkers, E., Bordas, P., Bozzo, E., Chenevez, J., Kouveliotou, C., & van der Horst, A. J. 2010, *The Astronomer’s Telegram*, 2940, 1
- Frank, J., King, A., & Raine, D. 1992, *Accretion power in astrophysics*. (Camb. Astrophys. Ser., Vol. 21)
- Galloway, D. K., Munro, M. P., Hartman, J. M., Psaltis, D., & Chakrabarty, D. 2008, *ApJS*, 179, 360
- Gehrels, N., et al. 2004, *ApJ*, 611, 1005
- Hameury, J.-M., Menou, K., Dubus, G., Lasota, J.-P., & Hure, J.-M. 1998, *MNRAS*, 298, 1048
- Hasinger, G. & van der Klis, M. 1989, *A&A*, 225, 79
- Heinke, C. O., et al. 2010, *ApJ*, 714, 894
- Homan, J., Kaplan, D. L., van den Berg, M., & Young, A. J. 2009, *ApJ*, 692, 73
- Kirsch, M. G., et al. 2005, *Proc. SPIE*, 5898, 22
- Lasota, J.-P. 2001, *New Astronomy Reviews*, 45, 449
- Lewin, W. H. G., van Paradijs, J., & van den Heuvel, E. P. J. 1997, *X-ray Binaries*, Edited by Walter H. G. Lewin and Jan van Paradijs and Edward P. J. van den Heuvel, pp. 674. ISBN 0521599342. Cambridge, UK: Cambridge University Press, January 1997.
- Lin, D., Remillard, R. A., & Homan, J. 2010, *ApJ*, 719, 1350
- Liu, Q. Z., van Paradijs, J., & van den Heuvel, E. P. J. 2007, *A&A*, 469, 807
- Lyu, M., Méndez, M., Sanna, A., Homan, J., Belloni, T., & Hiemstra, B. 2014, *MNRAS*, 440, 1165
- Maccarone, T. J. 2003, *A&A*, 409, 697
- Maccarone, T. J., & Coppi, P. S. 2003, *MNRAS*, 338, 189
- Matsuoka, M., et al. 2009, *PASJ*, 61, 999
- Matsuoka, M., & Asai, K. 2013, *PASJ*, 65, 26
- Meyer, F. 1984, *A&A*, 131, 303
- Mihara, T., et al. 2011, *PASJ*, 63, S623
- Mineshige, S., & Osaki, Y. 1983, *PASJ*, 35, 377
- Mineshige, S., & Osaki, Y. 1985, *PASJ*, 37, 1
- Mineshige, S., & Shields, G. A. 1990a, *ApJ*, 351, 47
- Mineshige, S., Tuchman, Y., & Wheeler, J. C. 1990b, *ApJ*, 359, 176
- Mitsuda, K., Inoue, H., Nakamura, N., & Tanaka, Y. 1989, *PASJ*, 41, 97
- Miyamoto, S., Kitamoto, S., Hayashida, K., & Egoshi, W. 1995, *ApJ*, 442, L13
- Muno, M. P., Fox, D. W., Morgan, E. H., & Bildsten, L. 2000, *ApJ*, 542, 1016
- Nakahira, S., et al. 2014, *The Astronomer’s Telegram*, 6250, 1
- Papitto, A., D’Ai, A., Motta, S., Riggio, A., Burderi, L. di Salvo, T., Belloni, T., & Iraria, R. 2011, *A&A*, 526, L3
- Revnivtsev, M., & Sunyaev, R. 2003, *A&A*, 399, 699
- Shih, I. C., Bird, A. J., Charles, P. A., Cornelisse, R., & Tiramani, D. 2005, *MNRAS*, 361, 602
- Shih, I. C., Charles, P. A., & Cornelisse, R. 2011, *MNRAS*, 412, 120
- Šimon, V. 2010, *A&A*, 513, 71
- Smak, J. 1982, *Acta Astronomica*, 32, 213
- Smak, J. 1983, *ApJ*, 272, 234
- Smak, J. 1984, *Acta Astronomica*, 34, 161
- Sugizaki, M., et al. 2011, *PASJ*, 63, S635
- Suzuki, M., et al. 2009, *The Astronomer’s Telegram*, 2360, 1
- Tang, J., Yu, W.-F., & Yan, Z. 2011, *Research in Astronomy and Astrophysics*, 11, 434
- Titarchuk, L., Seifina, E., & Frontera, F. 2013, *ApJ*, 767, 160
- Tomida, H., et al. 2013, *The Astronomer’s Telegram*, 5327, 1
- Tuchman, Y., Mineshige, S., & Wheeler, J. C. 1990, *ApJ*, 359, 164
- van der Klis, M. 1994, *ApJS*, 92, 511
- van Paradijs, J. 1996, *ApJ*, 464, L139
- Wen, L., Levine, A. M., Corbet, R. H. D., & Bradt, H. V. 2006, *ApJS*, 163, 372
- White, N. E., & Angelini, L. 2001, *ApJ*, 561, L101
- White, N. E., Stella, L., & Parmar, A. N. 1988, *ApJ*, 324, 363

- Wijnands, R., Altamirano, D., Heinke, C. O., Sivakoff, G. R.,
& Pooley, D. 2012, *The Astronomer's Telegram*, 4242, 1
- Yu, W., & Yan, Z. 2009, *ApJ*, 701, 1940